Mechanics of Materials 133 (2019) 102–110

Contents lists available at ScienceDirect

Mechanics of Materials

journal homepage: www.elsevier.com/locate/mechmat

Computational analysis of thermally induced stress concentration in structures with geometric constraints

Zhizhou Zhang, Kahraman Demir, Grace X. Gu*

Department of Mechanical Engineering, University of California, Berkeley, CA 94720-1740, USA

ARTICLE INFO

Keywords:
Thermal expansion
Finite element method
Materials design
Functionally graded materials

ABSTRACT

Fracture and fatigue life of an engineering component is highly sensitive to stress concentrations that can arise at sharp corners. Stress concentration can be caused by impact, pressure, and high temperatures, among other factors. High operating temperatures are common in internal combustion engines, batteries, computers, and additive manufacturing. In this work, we aim to provide systematic notch design guidelines for thin metallic plates subjected to strict geometrical boundary conditions under high temperatures. Computational analysis is used to investigate how geometrical configurations, near critical areas, affect the magnitude of thermally-induced stress and strain under the influence of uniform heating conditions. Results show that tuning the curvature of sharp corners can allow for the mitigation of potentially destructive thermally-induced stresses. Additionally, this study shows that the use of functionally graded materials (with varying values of coefficient of thermal expansion and modulus) can redistribute thermally-induced stresses, improving the structural performance of metallic materials in the presence of high temperature environments.

1. Introduction

Structural failure often arises due to undesired stress concentration caused by irregular shapes and cracks which greatly reduces the fatigue life of engineering components. As a result, much research has been dedicated to mitigating stress of structures, for example under static tension loading, by using design strategies like heterogeneity, hierarchy, and geometrical shapes (Jones et al., 2005; Das et al., 2005; Jang et al., 2004; Verho et al., 2018; Sanchez et al., 2005; Gu et al., 2016, 2017a,b,c). Geometrical shapes that have been studied include fillets or holes where material is added or removed at sharp corners to smooth the fringe and mitigate the stress concentration. Additionally, optimization algorithms and machine learning are also used to further hone in on many complex design problems with many variables (Brackett et al., 2011; Gaynor et al., 2014; Gu and Buehler, 2018; Gu et al., 2018a,b; Yeo et al., 2018). For instance, Sonmez worked on minimizing the maximum von Mises stress at the fillet of a shouldered plate by searching in a constrained domain the best boundary shape which is defined through multiple key points connected with spline curves (Sonmez, 2009). This method is used in many studies due to its adjustable boundary conditions and high accuracy under sufficient amount of key points (Schmid et al., 2005; Wu, 2005; Yoo et al., 2006). However, with their high accuracy comes a computational cost which signifies a tradeoff in design (Sonmez, 2007). In another work, Wu optimized a hole under tension loading by parameterizing the hole boundary with an analytical super-ellipse curve (Wu, 2009). Studies utilizing this method require fewer variables and still retain an effective optimization outcome (Van Miegroet and Duysinx, 2007; Pedersen, 2004; Phan and Phan, 1999). One challenge with these methods involves choosing the proper expression for the boundary curve with a reasonable number of variables (Wu, 2009). There are also researchers applying non-gradient optimization where they search for a fillet shape to reach uniform tangential stress along the boundary (Schnack and Spörl, 1986; Kaye and Heller, 2000; Waldman et al., 2001). This method appears to be both effective and efficient when no geometric constraint is enforced.

In addition to mechanical boundary conditions (tension, bending, or torsion), high temperature can also generate an unavoidable stress riser in applications such as internal combustion engines, batteries, computers and manufacturing. Many researchers have looked into the dynamic control factors to mitigate the residual stress and distortion caused by rapid local heating during welding and heat treatment process (Yang and Jung, 2007; Ren et al., 2014; Deo and Michaleris, 2003; Dong, 2005). Due to the complex coupling behavior between dynamic heating and deformation, the main research objective is analyzing the underlying reason and formation of the residual stress field instead of

* Corresponding author.
E-mail address: ggu@berkeley.edu (G.X. Gu).

https://doi.org/10.1016/j.mechmat.2019.03.006
Received 1 December 2018; Received in revised form 5 March 2019
Available online 08 March 2019

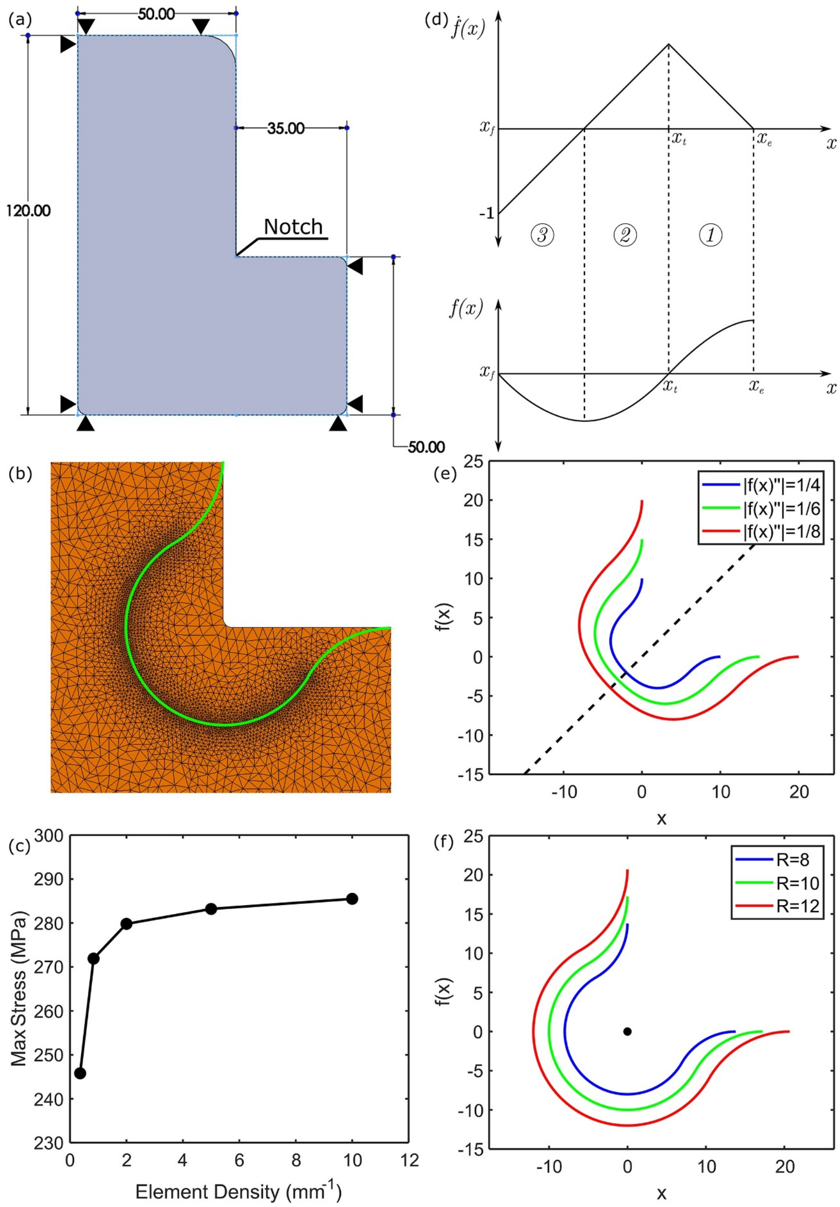

Fig. 1. (a) The thermal stress study setup for an L-shaped plate. All the dimensions are in millimeters. The edges highlighted with triangular marks are fixed. The heated temperature is set to 340 K with a reference room temperature of 298 K. (b) The converged mesh for a circular notch (R = 10 mm) filled with sacrificial material. The interface is highlighted with the green curve. (c) The mesh convergence study for a circular notch (R = 10 mm) filled with sacrificial material. (d) The slope and shape change of the notch profiles with constant concavity values. The slope is fixed at −1 on the left end and 0 on the right end of the profile. The absolute value of the slope change rate remains a constant throughout the profile. (e) Shapes of the notches with constant concavity values 1/4, 1/6 and 1/8 mm^{-1}. (f) Shapes of the notches with radius of curvature values of 8, 10, and 12 mm.

optimizing the entire dynamic system. The improved understanding will thus enable the tuning of temperature change rate, area of the heating zone, and heat path for longer service life. Additionally, researchers have also conducted static thermally-induced stress studies on particular structural materials. For instance, Ando et al. looked into design principals for tubesheets to mitigate the stress induced by high temperature and pressure (Ando et al., 2008). Weil and Koeppel analyzed the thermally-induced stress in the bonded compliant seal for fuel cells and window frames and proposed the potential design defects and improvements (Weil and Koeppel, 2008). However, there is a need to have a more thorough fundamental understanding of how geometrical configurations at critical areas affect structural response.

Due to the comprehensive studies on stress concentration induced by mechanical loadings in the past decades, it is natural for the scientific community to assume a highly similar effect from a thermal loading condition. However, it is of note that the two cases can be very different depending on how they are used in real world engineering structures. Mechanically-induced stress concentration usually occurs on a structure's load-bearing member which mostly undergoes a uniaxial or biaxial tensional loading, while thermally-induced stress concentration prevails in modern structures where compact assembly is required such as smart phones, vehicle engines and satellites, etc. In these scenarios, it is rational to regard them as complex compressive loading conditions that are highly correlated to the shapes of the bulk members and how their perimeters are bounded. Due to the great concern of yielding for metal materials, the huge distortional stress induced by these compressive loading conditions, which are currently not well understood, deserve a careful investigation. Thus, to fill this gap in literature, in this study we aim to systematically study the thermally-induced stress concentration pattern at a critical region of a loaded member under the most extreme boundary conditions and devise feasible methods to mitigate their effects. In this work, the stress concentration at the concave corner of thin metal plates under constant uniform temperature is studied. Different notch designs and their effects on mitigating the stress concentration will be simulated and discussed. Here, all notches will be created through removal of material to match the practical constraints from compact assembly (more details in Section 2). The entire shape of the plate and the relative location of the notch will be varied to examine the generality of the notch effect. Additionally, inspired by the new capabilities in additive manufacturing, we propose adding sacrificial materials (a second stronger material that will help reduce stress concentration) at the notch area as another

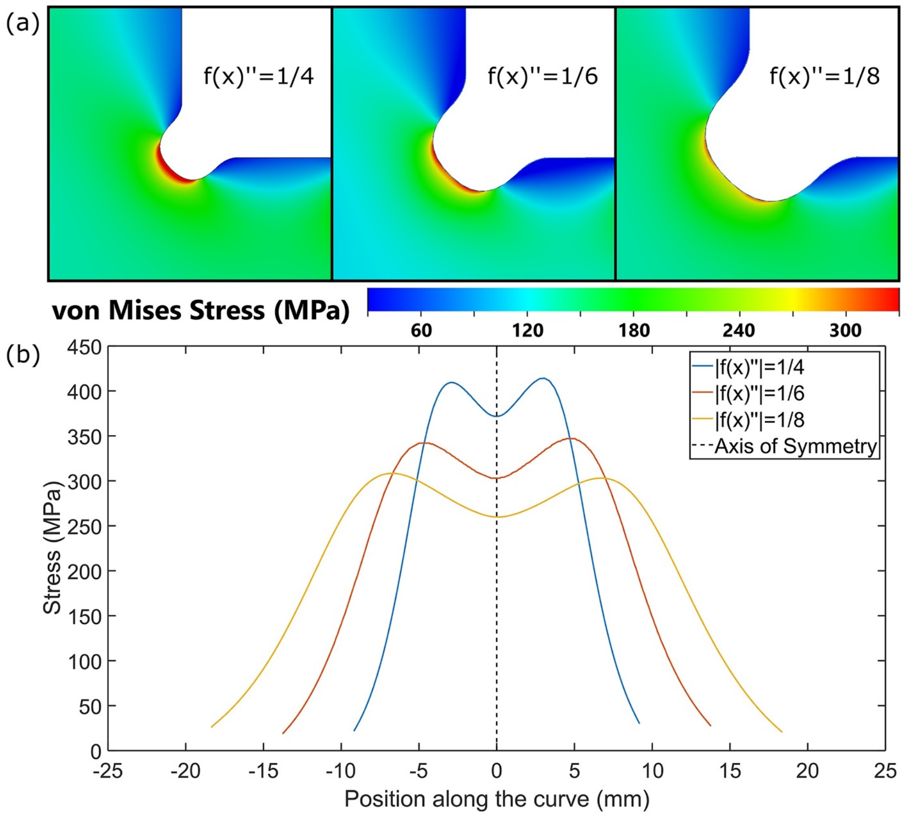

Fig. 2. (a) 2D simplified von Mises stress simulation results for notch designs with constant concavity values of 1/4, 1/6 and 1/8 mm^{-1}. (b) Stress distribution plots along the notch edge. It can be shown that two stress peaks exist around the axis of symmetry. As the concavity value decreases, the thermal stress is more distributed along the edge.

strategy. The finite element modeling method including model setup, boundary conditions, and material properties are defined in Section 2. Results and discussion of simulations are presented in Section 3. Section 4 will summarize the paper and discuss future work.

2. Materials and methods

2.1. Model setup and boundary conditions

The model problem studied in this work is a 2D L-shaped plate with a concave corner shown in Fig. 1. Plane stress conditions are assumed in the plate because the through thickness is small compared to the other dimensions, which is depicted in Fig. 1(a). The entire plate, initially at 23 °C, is subjected to an increased temperature of 70 °C, which is a common operating temperature for many electronic applications (Simons, and Chu, 2002; Liu et al., 2014). To magnify the thermally-induced stress, the plate is fixed at all edges except for those at the concave corner. We want to make a note here that the strict constraints may cause high stress concentration around the fixture corners which is not considered here since the focus of this work will be on the mitigation of thermally-induced stress concentration caused by the concave geometry. By omitting the thickness dimension (3 mm) which is less than 10% of the other dimensions, the element number is reduced by 90% with a negligible effect on the general trend of the von Mises stress profiles. In this study, the original shape of the plate given in Fig. 1(a) will be used as a geometric constraint. This implies that no modifications to the notch should bypass the perimeter of the original design. Similar geometrical restrictions are possible in compact assemblies such as in electronics and engines, or in extreme environments like those faced by space probes. In addition to generating different notch geometries, the use of sacrificial materials at the critical area will also be investigated. The sacrificial part will completely fill the subtracted area from the notch. The non-sacrificial part of the design will be denoted as the bulk material in the text.

The material considered here is a zinc-aluminum-magnesium alloy (preset from Solidworks software) with an elastic modulus of 85 GPa, Poisson's ratio of 0.3 and a coefficient of thermal expansion (CTE) of $2.74 \times 10^{-5}\,K^{-1}$. The material behavior is modeled as homogeneous, isotropic, and linear. As seen in Fig. 1(b), a representative mesh at the interface between the bulk material and the sacrificial material is chosen to balance computational efficiency and accuracy due to a discontinuity in material property which normally requires a higher mesh density than typical notches. A mesh convergence study is conducted and shown in Fig. 1(c) with less than 1% difference in von Mises stress values at the converged mesh density of 5 elements per millimeter along the notch edge. This paper will consider two main types of notch designs including Type 1 design with notches with constant slope change rates and Type 2 design with circular notches. To consider cases where material loss is undesirable, the potential of balancing peak stress and material loss is tested on both types of notches. Then, the effect of adding sacrificial material at the notch will also be investigated.

2.2. Type 1 design: notches with constant slope change rates

The first type of design considered has a constant changing rate of slope which is referred to as the concavity value $\ddot{f}(x) = c$ in this text. The concavity parameter is used to generate the notch profiles, $f(x)$, by first defining boundary conditions for the slope at the entrance of the notch and the end of the profile at the line of symmetry as seen in Fig. 1(d) where the half notch profile is divided into three regions. Regions 1 and 2 are positioned to satisfy the geometric constraint. All the three regions share the same length of $\frac{1}{c}$. The profiles are then mirrored across the symmetry line to reach the full cut-out notches shown in Fig. 1(e) at concavity values of c= 1/4, 1/6 and 1/8 mm^{-1}. The origin of $f(x)$ is defined to be the pre-existing corner of the plate without a notch (i.e. where the vertical and horizontal entrances to the notch intersect). Thus, the equations defining the profiles are shown below:

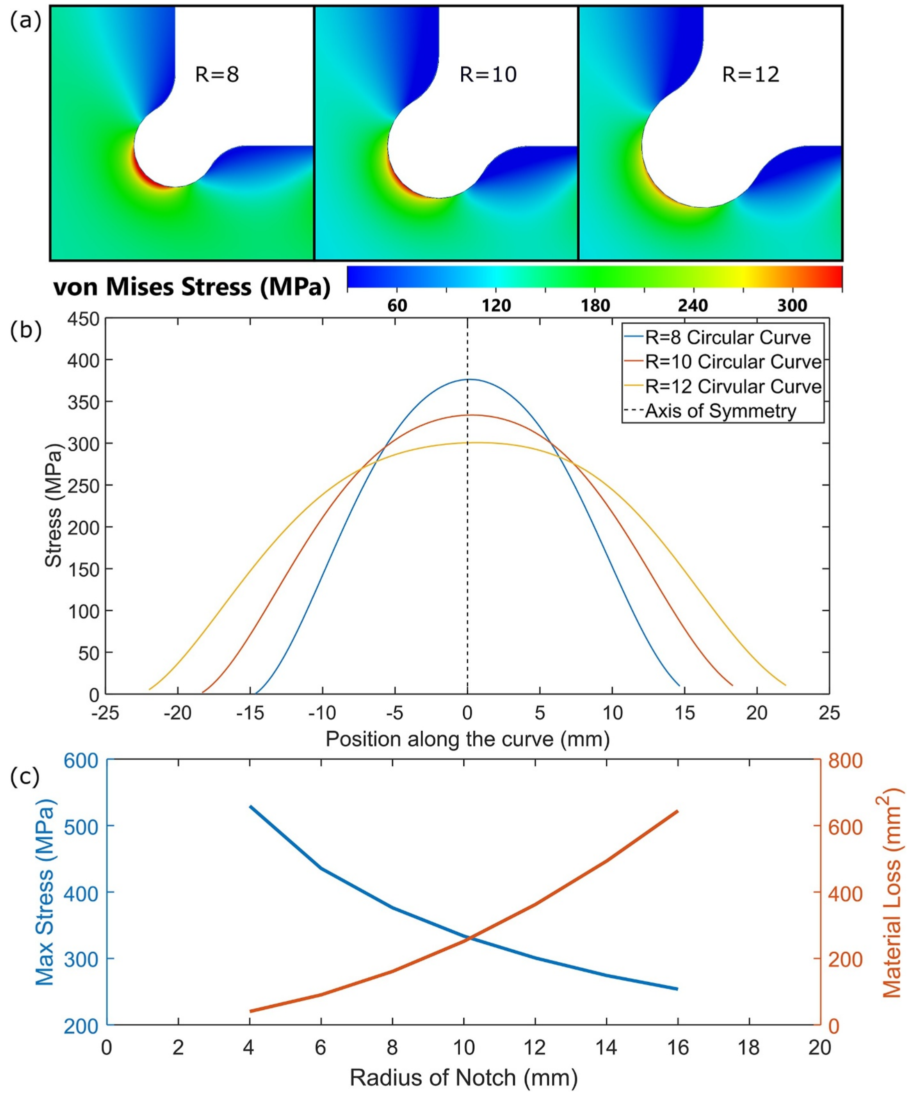

Fig. 3. (a) 2D simplified von Mises stress simulation results for circular notch designs with radius of 8, 10 and 12 mm. (b) Stress distribution plots along the notch edge. It can be shown that only a single stress peak exists at the axis of symmetry. As the radius increases, the thermal stress is more distributed along the edge. (c) The maximum von Mises stress along the edge of notches with radius varying from 4–16 mm. The corresponding area of material loss is also calculated.

$$f(x) = \begin{cases} \frac{c}{2}(x-x_t)^2 + (x-x_t) + x_f, & \text{for } x_f \le x \le x_t \\ -\frac{c}{2}(x-x_t)^2 + (x-x_t) + x_f, & \text{for } x_t \le x \le x_e \end{cases} \tag{1}$$

where c is the concavity value, $x_e = \frac{3}{c} - \frac{1}{2c}$ is the position of the entrance point, and $x_f = -\frac{1}{2c}$ is the point where the profile meets the line of symmetry, $y = x$.

2.3. Type 2 design: circular notches

In addition to the Type 1 designs, circular profiles (Type 2 design) are also investigated to relieve stresses at the notch. One common notch design for concave corners is a simple round fillet where material is added to form an arc that is tangent to the edges. However, this type of notch does not satisfy the geometry constraints introduced previously. Thus, the origin of the radius of curvature is placed at the 90° sharp corners shown in Fig. 1(f). Three notches are created with radii 8, 10 and 12 mm and any material inside of the circle is removed. The convex corners at the intersection of the circle and the edges are filleted with the same radius as of the circle to keep a constant radius of curvature throughout the entire notched curve.

3. Results

3.1. The effects of concavity (Type 1)

Three concavity values (1/4, 1/6 and 1/8 mm^{-1}) are considered for the notch curve. The concavity value is defined as the second derivative of a curve in the *xy*-plane which depicts the rate of change of the slope. This feature is chosen for its representation of the smoothness of the notch curve. The simulation results are shown in Fig. 2(a) as von Mises stress profiles that measure the yielding of ductile materials. Fig. 2(b) shows the von Mises stress distribution along the notch where the dashed line represents symmetry axis. The maximum effective stress along the notch for concavity values of 1/4, 1/6 and 1/8 mm^{-1} are 414.1, 347.0 and 308.3 MPa, respectively. Results show that as concavity decreases, maximum stress along the notch also decreases. Moreover, the stress tends to distribute more uniformly along the notch for smaller concavity values which leads us to believe that the larger notch size and length plays a critical role in the observed stress mitigation. While at the same time, the maximum stress values occur on both sides of the symmetry axis leading to two stress concentration peaks and a stress valley in the middle (Fig. 2(b)). To explain this result, the radius of curvature is calculated along the notch whose value decreases first and

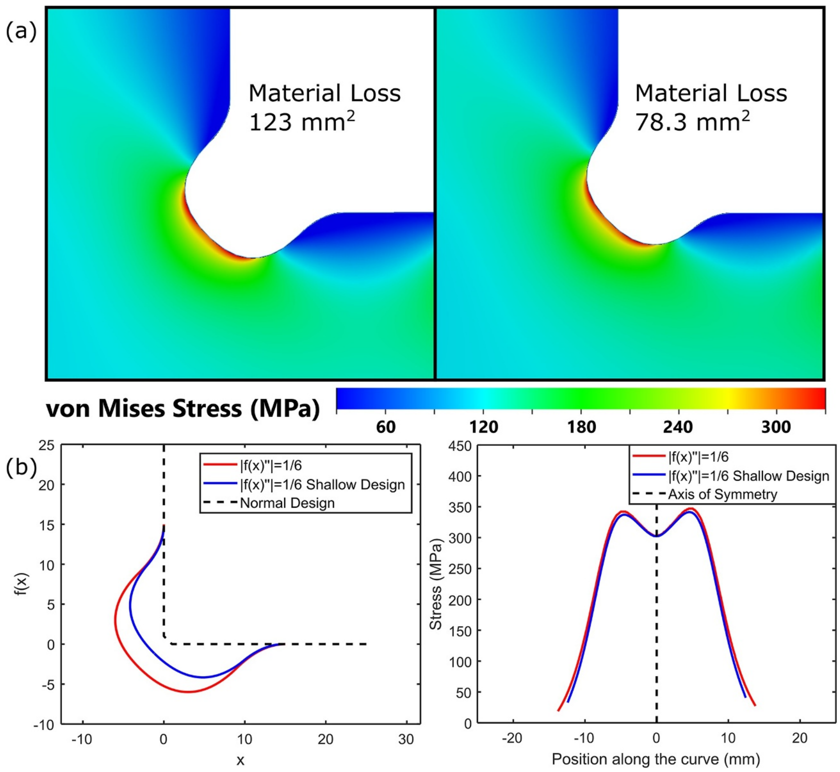

Fig. 4. (a) A comparison between 2D simplified von Mises stress simulation results for a 1/6 mm^{-1} concavity value notch design (Type 1 design) and a corresponding modified shallow design which reduces 36.3% of the material loss. (b) Stress distribution plots along the notch edge. Normal design indicates the geometry where no material is removed. The modified design (Shallow Design) has a similar stress distribution where the peaks are 1.64% lower than the original Type 1 design.

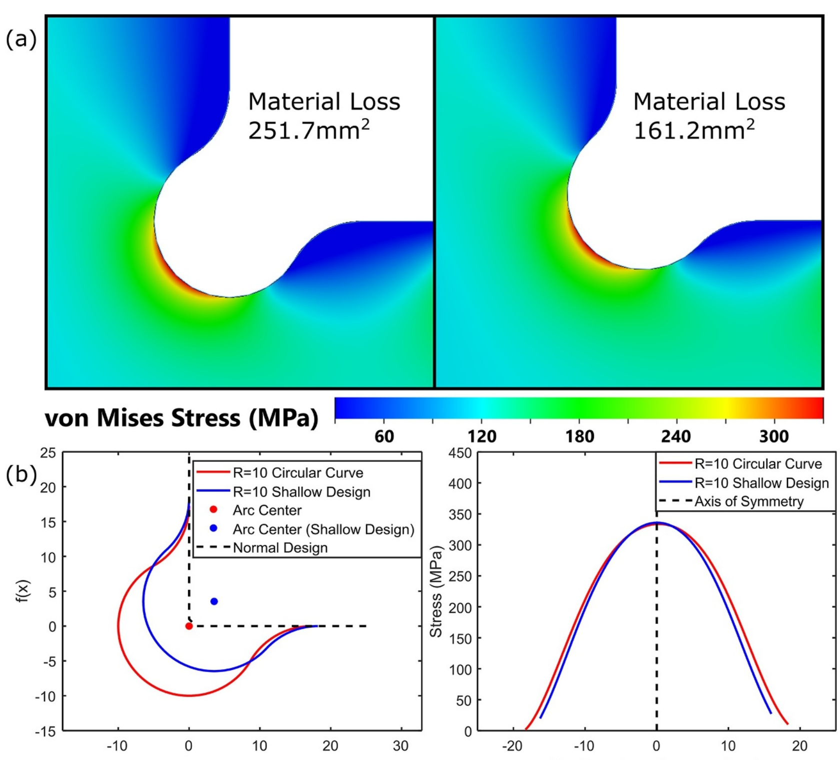

Fig. 5. (a) A comparison between 2D simplified von Mises stress simulation results for a circular design (Type 2 design) with a radius of 10 mm and a corresponding modified shallow design which reduces 36% of the material loss. (b) Stress distribution plots along the notch edge. Normal design indicates the geometry where no material is removed. The modified design (Shallow Design) has a similar stress distribution where the peak is 0.66% higher than the original Type 2 design.

increases to the maximum at the center of notch from region 2 to 3 (for details of the shape profile, refer to the Methods section). Thus, the two stress concentration peaks are closely related to the radius of curvature.

3.2. The effects of radius of curvature (Type 2)

Three radius of curvature values (8, 10, and 12 mm) are considered for the notch curve. As mentioned above, this feature is investigated for its possible influence on the stress distribution. The von Mises stress profiles are shown in Fig. 3(a). Fig. 3(b) shows the von Mises stress distribution along the notch with the dashed line representing the symmetry axis. The maximum effective stress along the notch for radii 8, 10 and 12 mm are 376.3, 333.7 and 300.7 MPa where the stress along the notch decreases as the circle gets larger. To further validate the

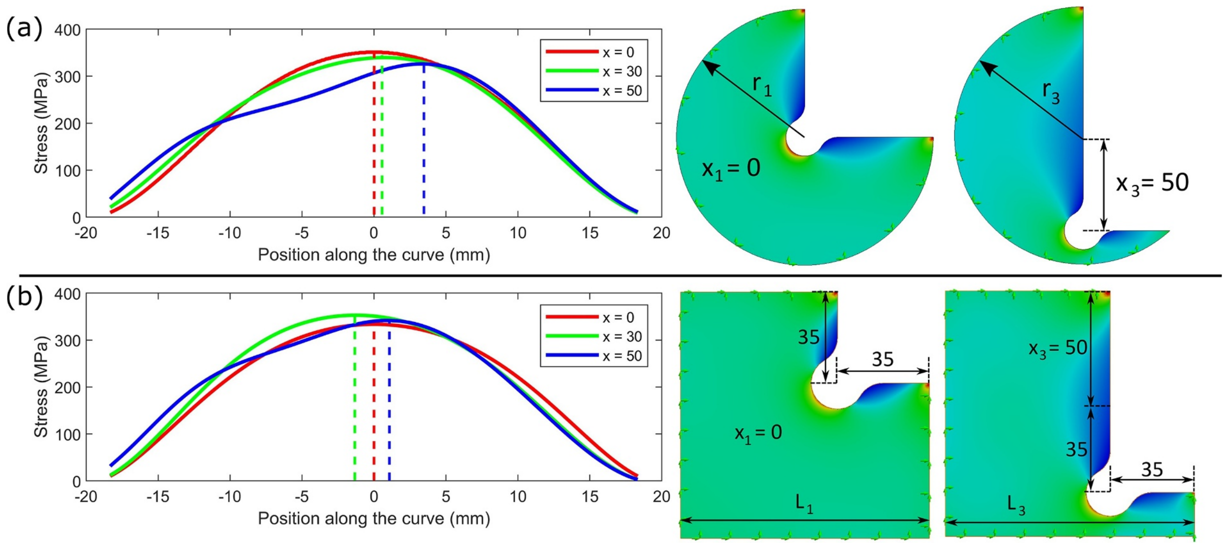

Fig. 6. Investigation on the stress profiles of different mass distributions around the notch. The shapes and their alterations have equivalent mass. (a) Circular base shape (b) rectangular base shape. Boundary conditions are unchanged. x is the offset dimension where when $x = 0$, the shape is symmetrical and where $x > 0$, it is unsymmetrical. Three values of x were chosen: 0, 30, and 50 mm. Vertical lines show maximum stress locations.

hypothesis, the peak effective stress of notches with radius varying from 4–16 mm is simulated and plotted in Fig. 3(c). The corresponding area of material loss is calculated to better quantify the notch size. As expected, the stress becomes more distributed as the radius of the notch increases which proves the necessity of the notch size in mitigating thermally-induced stress concentration. However, the mitigation effect decays as the radius keep increasing. This indicates the existence of an optimized radius under certain practical cases. Furthermore, the stress distribution gives a different pattern compared with notches using constant concavity values. For circular notches with a constant radius of curvature, the maximum stress occurs at the center of symmetry where the stress rises or falls monotonically before or after the peak. Hence, the two peaks observed from Type 1 notches are likely to be caused by the local minimum radius of curvature on both sides of the symmetrical axis, and the local stress minimum is the result of a radius maximum at the center. It should be noted that although radius can affect the thermally-induced stress concentration to some extent, the extreme stress values do not occur at the exact same position as the extreme radius values. This correlation between radius of curvature and stress concentration is consistent with Neuber's Fade-away Law (Neuber, 1958). However, due to the complex boundary conditions of this thermally-loaded plate, there can be multiple correlated factors besides radius affecting the stress concentration at the notch. Thus, the effect of the notch size and entire plate shape while keeping other features fixed will be examined.

3.3. Reduction of material loss

As mentioned in the Methods section, material addition at the notch is not allowed under a geometric constraint which is determined by the original bulk shape perimeter. The previous section shows that larger notches tend to have more uniform stress distribution and lower peak stress (Fig. 3(c)). However, there exist cases where material reduction is undesirable due to a more complex manufacturing process or a tradeoff in product property like battery capacity which is highly related to its volume (Bar-cohen, 1992). To explore the tradeoff between stress mitigation and material loss, shape modifications are explored. For the Type 1 notch with a concavity value of $1/6\ \mathrm{mm}^{-1}$, the length of region 1 and 2 is reduced by 2 mm (for details of the shape profile, refer to the Methods section) which makes the notch shallower as shown in Fig. 4(a) while keeping the shape within the constraints. As seen in Fig. 4(b) the modified notch has a similar stress distribution where the peak stress is even 1.64% lower than the original notch. Furthermore, the material loss is reduced by 36.3% with the modified design.

A similar modification is performed on the Type 2 notch with a radius of curvature of 10 mm. The origin of the radius was moved out 5 mm along the axis of symmetry with the sharp corners filleted accordingly as shown in Fig. 5(a). This modification creates a shallower version of the circular notch while retaining its geometric features and practical constraints. Results show a similar stress distribution with a peak stress 0.66% higher than the original circular notch as seen in Fig. 5(b). In this case, a material loss reduction of 36% is achieved.

These results validate the assumption that lower thermally-induced stress concentration is not necessarily caused by larger notch sizes. Rather, the distribution is more influenced by the radius of curvature and length of the critical region of the notch. This critical region refers to region 3 in Type 1 notches and the center arc in Type 2 notches where stress peaks occur. However, the modifications described above mainly focus on regions 1 and 2 in Type 1 notches and the fillet corners in Type 2 notches which are necessary for practical constraints but are slightly stressed. This reveals the possibility of tailoring the notch to obtain a minimized stress concentration and material loss.

3.4. Variations in mass distribution

In this section, different distributions of mass around the notch are investigated for their effect on the stress profile along the notch. As seen in Fig. 6, two base shapes (circle and square) are selected and a notch radius of 10 mm is used. The different shapes were generated by offsetting the notch by x mm while keeping the area constant at $7750\ \mathrm{mm}^2$. Three values of x were chosen: 0, 30, and 50 mm. An x value of zero results in a symmetrical shape for which the stress profile is also symmetrical about the zero position along the notch, indicated by the red dotted vertical line on the plots in Fig. 6. When x is a non-zero value the shape is no longer symmetrical, and this results in an unsymmetrical stress profile that can be seen by the offset vertical lines in Fig. 6. This is caused by a larger unrestricted boundary on one side of the shape resulting in an unbalanced relief of material flow.

3.5. Addition of sacrificial material

In previous sections, material is removed from the notch to mitigate the thermally-induced stress concentration which creates empty space that is likely to be unused in real applications. Thus, we aim to look at

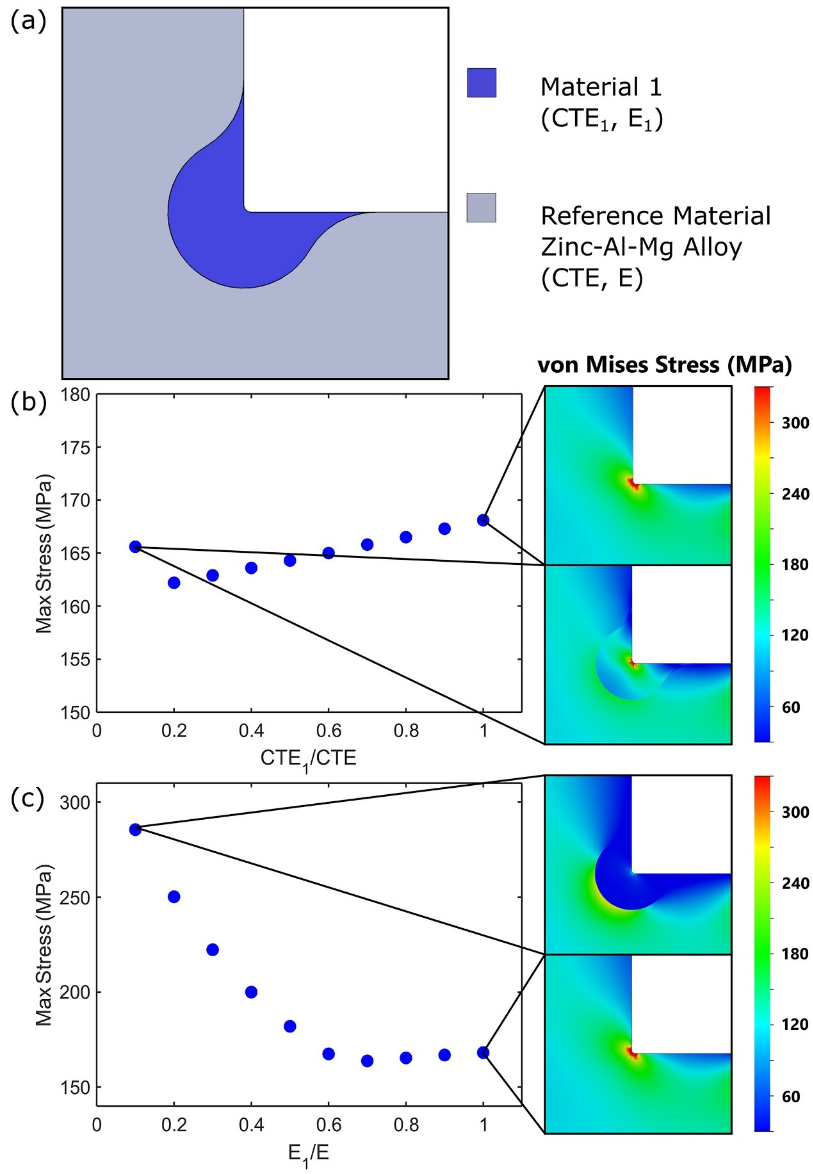

Fig. 7. (a) A circular notch design (10 mm radius) filled with sacrificial material highlighted in blue. Different coefficient of thermal expansion (CTE_1) and modulus (E_1) are assigned to the sacrificial material. (b) Maximum von Mises stress around the notch in the bulk material at different CTE_1 values. The simulation stress profile results at thermal expansion coefficient ratio (CTE_1/CTE) of 0.1 and 1 are shown. (c) Maximum von Mises stress around the notch in the bulk material at different E_1 values. The simulation stress profile results at modulus ratio (E_1/E) of 0.1 and 1 are shown.

the possibility of utilizing this space to further reduce the stress. Additional material is added to completely fill the gap between the notch and the boundaries. The hypothetical material in this area is defined as a sacrificial material which we assume will not yield or fail. This method is inspired by the development of additive manufacturing which allows multi-material designs with complex geometries (Libonati et al., 2016; Gao et al., 2015, 2017a,b,c; Gibson et al., 2015; Guo and Leu, 2013; Huang et al., 2015). The materials are assumed to be perfectly bonded at the interface. Different modulus (E), coefficient of thermal expansion (CTE) and Poisson's ratio are assigned to the sacrificial material as shown in Fig. 6(a) and the max von Mises stress in the bulk material (not sacrificial material) around the notch is investigated. The Type 2 notch geometry with a radius of 10 mm is used for this case study.

First, the coefficient of thermal expansion of the sacrificial material (CTE_1) is taken as the varying input parameter while both materials share the same modulus. A ratio of CTE_1 to CTE (the bulk material CTE) is considered here. It can be seen from the stress map in Fig. 7(b) that a high stress concentration occurs at the sharp concave corner of the sacrificial material which is acceptable for its irrelevance to the function of the bulk part. The benefit of adding sacrificial material is the large reduction in the max von Mises stress around the circular notch which gradually decreases as CTE_1 gets smaller until a ratio (CTE_1/CTE) of 0.2 is reached where a rapid stress rise is observed. The optimum stress at a CTE_1/CTE ratio of 0.2 is only 162.2 MPa which is around 50% of the peak stress (333.7 MPa) without the sacrificial material.

Next, the modulus of the sacrificial material (E_1) was taken as the varying parameter with CTE_1 set equal to the coefficient of thermal expansion of the bulk material (reference CTE). Similarly, this parameter is divided by the modulus of the bulk material to get a normalized ratio of E_1/E. Results show that the max von Mises stress around the notch has a similar trend as in Fig. 7(c) except that the optimum occurs at a modulus ratio of 0.6. The rapid climb can still be observed when the sacrificial material gets even softer. The corresponding optimum stress is 163.8 MPa which is again close to 50% of the peak stress without the sacrificial material.

A third important property of an isotropic elastic material is the Poisson's ratio. Simulations are carried out similarly as for CTE and E

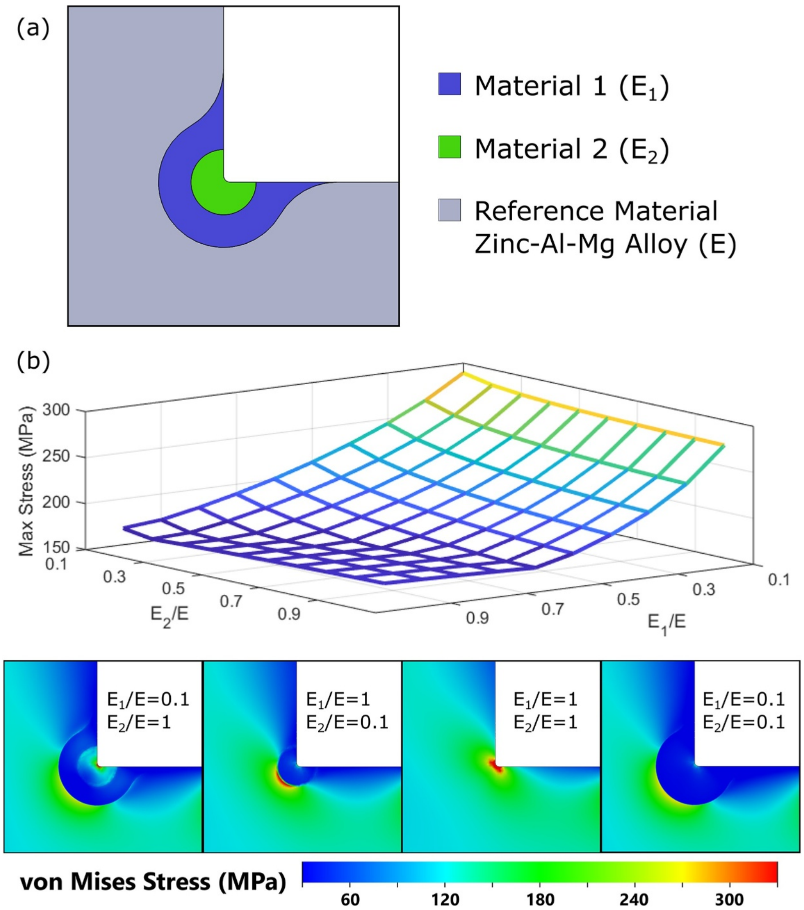

Fig. 8. (a) A circular notch design (10 mm radius) filled with two different sacrificial materials highlighted in blue and green. Each of them covers a radius of 5 mm. Different modulus E_1 and E_2 are assigned to the two sacrificial materials. (b) Maximum von Mises stress around the notch in the bulk material at different combinations of E_1 and E_2 values. The modulus ratios (E_1/E and E_2/E) vary from 0.1 to 1 with an increment of 0.1. The simulation stress profile results at four different cases are shown.

except that the Poisson's ratio of the sacrificial material is not normalized to the bulk material due to its dimensionless nature. The range of the Poisson's ratio is chosen to be between 0.2–0.4, which covers most of the typical metals. Our results show that the peak stress at the notch stays within 168 ± 0.7 MPa throughout the Poisson's ratio variation range. This indicates that tuning sacrificial material's Poisson's ratio does not have a large effect on stress concentration compared with tuning the properties of modulus and coefficient of thermal expansion.

To address the thermally-induced stress reduction caused by the sacrificial material, the source of the stress concentration is investigated. Since the test object is fixed at most of its margin as discussed in the Methods section, the thermal expansion is forced toward the concave notch in which direction the object is free to move. As a result, the notch area which would be expanded if the whole object is free to swell is squeezed and thus shrunk. A smaller notch perimeter will compress the material in the tangential direction and drive up the corresponding compressive stress. The existence of the sacrificial material will create a resistant compressive stress on the radial direction which is undesirable. However, this will restrict the change in the notch perimeter and thus mitigate the tangential compression. Hence, it is possible to reach some optimum thermally-induced stress concentration on the notch that is much smaller compared to an empty notch if the properties of the sacrificial material are carefully chosen.

3.6. Discussion and future work

The previous tests reveal that filling the notch with sacrificial material can distribute the thermally-induced stress and mitigate the stress concentration which is beneficial assuming the added material is not vulnerable to yielding or failure. And the mitigation highly depends on the property relation between the bulk material and the sacrificial material. Inspired by these results, we also conduct a 3D design study where the notch is filled with more than one sacrificial material, termed a functional-graded material. Fig. 8(a) shows the setup for the notch with two different sacrificial materials. Material 2 occupies a circular region at a radius of 5 mm and material 1 fills the rest of the Type 2 notch at a radius of 10 mm. Different modulus (E_1 and E_2) are assigned to the sacrificial materials while all three parts share the same coefficient of thermal expansion. The maximum von Mises stress and the stress profiles under four specific cases are shown in Fig. 8(b) where the horizontal arises represent the modulus ratios. The rapid and slow stress climb at low and high modulus ratios, respectively, are consistent with the single sacrificial material results. From the figure, it is observed that multiple E_1 and E_2 combinations achieve the optimum stress value around 163 MPa. The stress valley formed by these combinations can be approximated by the following relationship: $\frac{E_1}{E} + \frac{E_2}{2E} = 1$. This leads to a potentially existing analytical model for adding gradient material for reduction of thermally-induced stress at a concave notch.

In this paper, we observe how various shapes and different materials affect stress concentration of irregularly shaped materials. Thermally-induced stress results show that there is a possibility for optimal combinations of these features for the design. Future work includes performing topology optimization analysis for determining optimum shapes and materials for mitigating thermally-induced stress concentration of materials.

4. Conclusions

In this work, we aim to provide systematic notch design guidelines for thin metallic plates subjected to strict geometrical boundary conditions under high temperatures. Type 1 (constant concavity) and 2 (circular) notch designs are tested at a 90° concave corner under a geometric constraint to mitigate the thermally-induced stress concentration of a heated object whose boundaries are fixed. Results show a high correlation between the stress distribution pattern along the notch edge and its radius of curvature. Due to the stress being primarily related to the curvature of the notch, the depth at which the notch is made does not greatly affect the magnitude of the thermally-induced stress. Large stresses only appear in regions of the notch that are concave and have small radius of curvature. Hence, a shallower notch could be favorable to minimize material removal. The effects of mass distribution were also investigated, and results showed that the stress profile depended on the symmetry of the base shape. Additionally, the stress concentration of the notch is also explored when it is filled with sacrificial materials within the geometric constrains. The coefficient of thermal expansion and the modulus of the sacrificial material can be tuned to reduce the stress peak along the notch by 50%. Moreover, when there are two different kinds of sacrificial materials, the minimum von Mises stress can be achieved with a series of material property combinations. This result shows the potential in minimizing thermally-induced stress with functionally-graded materials at the notch. An extension to this work includes performing topology optimization analysis for determining optimum shapes and materials for mitigating thermally-induced stress concentration of notches.

Acknowledgement

The authors acknowledge support from the Regents of the University of California, Berkeley.

References

Ando, M., Takasho, H., Kawasaki, N., Kasahara, N., 2008. Stress mitigation design of tubesheets with consideration of. In: ASME 2008 Pressure Vessels and Piping Conference, pp. 1–10.

Bar-Cohen, A., 1992. State-of-the-Art and Trends in the Thermal Packaging of Electronic Equipment. J. Electronic Packaging 114 (3), 257. https://doi.org/10.1115/1.2905450.

Brackett, D., Ashcroft, I., Hague, R., 2011. In: Proceedings of the Solid Freeform Fabrication Symposium, pp. 348–362.

Das, R., Jones, R., Xie, Y.M., 2005. Design of structures for optimal static strength using ESO. Eng. Fail. Anal. 12 (1), 61–80. https://doi.org/10.1016/j.engfailanal.2004.05.002.

Deo, M.V., Michaleris, P., 2003. Mitigation of welding induced buckling distortion using transient thermal tensioning. Sci. Technol. Weld. Join. 8 (1), 49–54. https://doi.org/10.1179/136217103225008919.

Dong, P., 2005. Residual stresses and distortions in welded structures: a perspective for engineering applications. Sci. Technol. Weld. Join. 10 (4), 389–398. https://doi.org/10.1179/174329305X29465.

Gao, W., Zhang, Y., Ramanujan, D., Ramani, K., Chen, Y., Williams, C.B., Wang, C.C.L., Shin, Y.C., Zhang, S., Zavattieri, P.D., 2015. The Status, challenges, and future of additive manufacturing in engineering. CAD Comput. Aided Des. 69, 65–89. https://doi.org/10.1016/j.cad.2015.04.001.

Gaynor, A.T., Meisel, N.A., Williams, C.B., Guest, J.K., 2014. Multiple-material topology optimization of compliant mechanisms created via PolyJet three-dimensional printing. J. Manuf. Sci. Eng. 136 (6), 061015. https://doi.org/10.1115/1.4028439.

Gibson, I., Rosen, D., Stucker, B., 2015. 3D Printing, Rapid Prototyping, and Direct Digital Manufacturing, second ed. Additive Manufacturing Technologies. https://doi.org/10.1007/978-1-4939-2113-3.

Gu, G.X., Buehler, M.J., 2018. Tunable mechanical properties through texture control of polycrystalline additively manufactured materials using adjoint-based gradient optimization. Acta Mech. (July), 1–12. https://doi.org/10.1007/s00707-018-2208-1.

Gu, G.X., Chen, C.-T., Buehler, M.J., 2018a. De novo composite design based on machine learning algorithm. Extreme Mech. Lett. 18 (January), 19–28. https://doi.org/10.1016/J.EML.2017.10.001.

Gu, G.X., Chen, C.-T., Richmond, D.J., Buehler, M.J., 2018b. Bioinspired hierarchical composite design using machine learning: simulation, additive manufacturing, and experiment. Mater. Horiz. 5 (5), 939–945. https://doi.org/10.1039/C8MH00653A.

Gu, G.X., Libonati, F., Wettermark, S.D., Buehler, M.J., 2017a. Printing nature: unraveling the role of nacre's mineral bridges. J. Mech. Behav. Biomed. Mater. 76 (December), 135–144. https://doi.org/10.1016/J.JMBBM.2017.05.007.

Gu, G.X., Takaffoli, M., Buehler, M.J., 2017b. Hierarchically enhanced impact resistance of bioinspired composites. Adv. Mater. 29 (28), 1–7. https://doi.org/10.1002/adma.201700060.

Gu, G.X., Takaffoli, M., Hsieh, A.J., Buehler, M.J., 2016. Biomimetic additive manufactured polymer composites for improved impact resistance. Extreme Mech. Lett. 9 (December), 317–323. https://doi.org/10.1016/j.eml.2016.09.006.

Gu, G.X., Wettermark, S., Buehler, M.J., 2017c. Algorithm-driven design of fracture resistant composite materials realized through additive manufacturing. Addit. Manuf. 17 (October), 47–54. https://doi.org/10.1016/j.addma.2017.07.002.

Guo, N., Leu, M.C., 2013. Additive manufacturing: technology, applications and research needs. Front. Mech. Eng. 8 (3), 215–243. https://doi.org/10.1007/s11465-013-0248-8.

Huang, Y., Leu, M.C., Mazumder, J., Donmez, A., 2015. Additive manufacturing: current state, future potential, gaps and needs, and recommendations. J. Manuf. Sci. Eng. 137 (1), 014001. https://doi.org/10.1115/1.4028725.

Jang, G.W., Kim, Y.Y., Choi, K.K., 2004. Remesh-free shape optimization using the Wavelet-Galerkin method. Int. J. Solids Struct. 41 (22–23), 6465–6483. https://doi.org/10.1016/j.ijsolstr.2004.05.010.

Jones, R., Peng, D., Chaperon, P., Pitt, S., Abramson, D., Peachey, T., 2005. Structural optimisation with damage tolerance constraints. Theor. Appl. Fract. Mech. 43 (1), 133–155. https://doi.org/10.1016/j.tafmec.2004.12.009.

Kaye, R., Heller, M., 2000. Investigation of shape optimization for the design of life extension options for an F/A-18 Airframe FS 470 Bulkhead. J. Strain Anal. Eng. Des. 35 (6), 493–505. https://doi.org/10.1243/0309324001514251.

Libonati, F., Gu, G.X., Qin, Z., Vergani, L., Buehler, M.J., 2016. Bone-inspired materials by design: toughness amplification observed using 3d printing and testing. Adv. Eng. Mater. 18 (8), 1354–1363. https://doi.org/10.1002/adem.201600143.

Liu, N., Lu, Z., Zhao, J., Mcdowell, M.T., Lee, H.W., Zhao, W., Cui, Y., 2014. A pomegranate-inspired nanoscale design for large-volume-change lithium battery anodes. Nat. Nanotechnol. 9 (3), 187–192. https://doi.org/10.1038/nnano.2014.6.

Miegroet, L.V., Duysinx, P., 2007. Stress concentration minimization of 2D filets using X-FEM and level set description. Struct. Multidiscip. Optim. 33 (4–5), 425–438. https://doi.org/10.1007/s00158-006-0091-1.

Neuber, H., 1958. Einführung und übersicht. Kerbspannungslehre. Springer Berlin Heidelberg, Berlin, Heidelberg, pp. 1–7. https://doi.org/10.1007/978-3-642-53069-2_1.

Pedersen, P., 2004. Design study of hole positions and hole shapes for crack tip stress releasing. Struct. Multidiscip. Optim. 28 (4), 243–251. https://doi.org/10.1007/s00158-004-0416-x.

Phan, A.V., Phan, T.N., 1999. Structural Shape Optimization System Using the Two-Dimensional Boundary Contour Method. Archive of Applied Mechanics 69 (7), 481-89. https://doi.org/10.1007/s004190050236.

Ren, X.D., Zhan, Q.B., Yuan, S.Q., Zhou, J.Z., Wang, Y., Ren, N.F., Sun, G.F., et al., 2014. A finite element analysis of thermal relaxation of residual stress in laser shock processing Ni-based alloy GH4169. Mater. Des. 54, 708–711. https://doi.org/10.1016/j.matdes.2013.08.054.

Sanchez, C., Arribart, H., Guille, M.M.G., 2005. Biomimetism and bioinspiration as tools for the design of innovative materials and systems. Nat. Mater. 4 (4), 277–288. https://doi.org/10.1038/nmat1339.

Schmid, F., Hirschen, K., Meynen, S., Schäfer, M., 2005. An enhanced approach for shape optimization using an adaptive algorithm. Finite Elem. Anal. Des. 41 (5), 521–543. https://doi.org/10.1016/j.finel.2004.07.005.

Schnack, E., Uwe, S., 1986. A Mechanical Dynamic Programming Algorithm for Structure Optimization. International Journal for Numerical Methods in Engineering 23 (11), 1985–2004. https://doi.org/10.1002/nme.1620231103.

Simons, R.E., Chu., R.C., 2002. Application of Thermoelectric Cooling to Electronic Equipment: A Review and Analysis. In: Sixteenth Annual IEEE Semiconductor Thermal Measurement and Management Symposium (Cat. No.00CH37068). IEEE, pp. 1–9. https://doi.org/10.1109/stherm.2000.837055.

Sonmez, F.O., 2007. Shape optimization of 2D structures using simulated annealing. Comput. Methods Appl. Mech. Eng. 196 (35–36), 3279–3299. https://doi.org/10.1016/j.cma.2007.01.019.

Sonmez, F.O., 2009. Optimal shape design of shoulder fillets for flat and round bars under various loadings. Proc. Inst. Mech. Eng. Part C 223 (8), 1741–1754. https://doi.org/10.1243/09544062JMES1457.

Verho, T., Karppinen, P., Gröschel, A.H., Ikkala, O., 2018. Imaging inelastic fracture processes in biomimetic nanocomposites and nacre by laser speckle for better toughness. Adv. Sci. 5 (1). https://doi.org/10.1002/advs.201700635.

Waldman, W., Heller, M., Chen, G.X., 2001. Optimal free-form shapes for shoulder fillets in flat plates under tension and bending. Int. J. Fatigue 23 (6), 509–523. https://doi.org/10.1016/S0142-1123(01)00011-1.

Weil, K.S., Koeppel, B.J., 2008. Thermal stress analysis of the planar sofc bonded compliant seal design. Int. J. Hydrog. Energy 33 (14), 3976–3990. https://doi.org/10.1016/j.ijhydene.2007.11.008.

Wu, Z., 2005. An efficient approach for shape optimization of components. Int. J. Mech. Sci. 47 (10), 1595–1610. https://doi.org/10.1016/j.ijmecsci.2005.06.012.

Wu, Z., 2009. Optimal hole shape for minimum stress concentration using parameterized geometry models. Struct. Multidiscip. Optim. 37 (6), 625–634. https://doi.org/10.1007/s00158-008-0253-4.

Yang, Y.P., Jung, G., 2007. Advancement in prediction and control of welding residual stress and distortion. Mater. Sci. Forum 539–543, 3943–3948. https://doi.org/10.4028/www.scientific.net/MSF.539-543.3943.

Yeo, J., Jung, G.S., Martín-Martínez, F.J., Ling, S., Gu, G.X., Qin, Z., Buehler, M.J., 2018. Materials-by-design: computation, synthesis, and characterization from atoms to structures. Phys. Scripta 93 (5). https://doi.org/10.1088/1402-4896/aab4e2.

Yoo, H.H., Cho, J.E., Chung, J., 2006. Modal analysis and shape optimization of rotating cantilever beams. J. Sound Vib. 290 (1–2), 223–241. https://doi.org/10.1016/j.jsv.2005.03.014.